Enantioselective photoenzymatic C(sp^3)-H functionalization via single-electron oxidation of carbanions

Jin Zhu[1,2,6], Qiaoyu Zhang[3,6], Tao Gu[2,6], Binbin Chen[2], Mingzhe Ma[2], Xiaoyu Wang[3], Xiao Liu[2], Mingjie Ma[2], Binju Wang[3*], and Yajie Wang[2,4,5*]

[1]School of Materials Science and Engineering, Zhejiang University, Hangzhou, Zhejiang 310058, China.

[2]School of Engineering, Westlake University, Hangzhou 310030, China.

[3]Key Laboratory of Theoretical and Computational Chemistry, College of Chemistry and Chemical Engineering, Xiamen University, Xiamen 361005, China.

[4]School of Life Science, Westlake University, Hangzhou 310030, China.

[5]Westlake Center of Synthetic Biology and Integrated Bioengineering, Westlake University, Hangzhou 310030, China.

[6]These authors contributed equally: Jin Zhu, Qiaoyu Zhang, and Tao Gu.

*Corresponding author Emails: wangbinju2018@xmu.edu.cn; wangyajie@westlake.edu.cn

Abstract

C-H functionalization provides unparalleled benefits for the late-stage modification of complex molecules. In recent years, photocatalysis has progressed significantly due to its mild conditions, sustainability and selectivities. Current mechanisms for photocatalytic C-H functionalization primarily involve direct single-electron oxidation and direct hydrogen atom transfer (*d*-HAT) by radicals, both of which are invalid for the functionalization of highly electron-deficient C(sp^3)-H bonds. Here, we developed a cooperative photoenzymatic system consisting of a flavin-dependent 'ene'-reductase (ER) and an exogenous photocatalyst fluorescein (FI) to achieve enantiodivergent functionalization of electron-deficient C(sp^3)-H bonds. Mechanistic studies revealed a novel pathway for radical intermediate formation via excited-state FI^*-induced single-electron oxidation of carbanions under alkaline conditions. The overall catalytic efficiency is enhanced by the electron transfer (ET) between FMN_{ox} and $FI^{-\bullet}$, while the stereoselectivity is controlled by ERs through enantioselective hydrogen atom transfer (HAT). This suggests that thermodynamically unfavorable single-electron oxidation of highly electron-deficient species can occur through ion-to-radical conversion. We anticipate that our novel mode of photoenzymatic catalysis will inspire new pathways for generating free radical intermediates and foster innovative strategies for achieving photoenzymatic new-to-nature reactions.

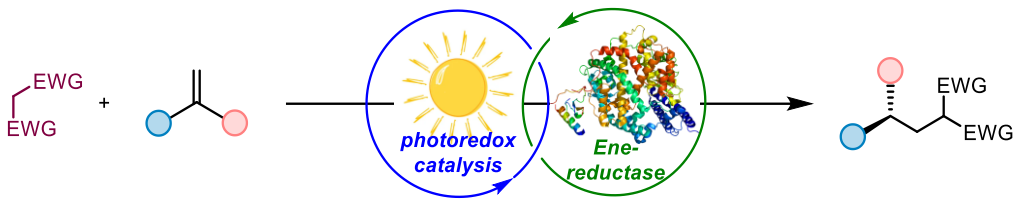

- Enantioselective functionalization of electron-deficient C(sp^3)-H bonds
- Radical formation by single-electron oxidation of carbanion
- The synergistic action of fluorescein and enzyme
- Enantiodivergent synthesis

Introduction

C-H functionalization, particularly C(sp^3)-H, is pivotal in synthetic chemistry for its efficiency in constructing complex molecules from simple precursors, high atom economy, and versatility in late-stage modification of diverse precursors in pharmaceuticals and materials science.[1,2] Visible-light photoredox catalysis has rapidly emerged as a robust strategy in this context due to its catalytic versatility, mild conditions, sustainability, and high selectivities.[3-6] Photocatalytic C(sp^3)-H functionalization primarily relies on two mechanisms to generate carbon-centered radicals: direct single-electron oxidation of C-H bonds[4] and direct hydrogen atom transfer (*d*-HAT) (Fig. 1a)[5].The former requires electron-rich, easily oxidizable C-H bonds[7,8], while the latter depends on the hydrogen abstraction by polarity-matched radical species[3,9-12]. Both mechanisms pose challenges for selective electron-deficient C(sp^3)-H bonds functionalization. In addition, asymmetric C(sp^3)-H functionalization via hydrogen atom transfer (HAT) with prochiral radicals presents challenges, partly due to the small size of the H atom and the early transition state associated with this process.[13,14] Therefore, photocatalysis can have great potential in the enantioselective functionalization of electron-deficient C(sp^3)-H bonds, but it also presents substantial challenges.

Recent advancements in photoenzymatic catalysis have shown remarkable enantioselectivity in the asymmetric HAT of prochiral radicals[15-30]. The radicals are produced either through the single-electron reduction of an electron-donor-acceptor (EDA) complex[15-26] or via the single-electron oxidation of electron-rich precursors[27-30].

Notably, these methods have been successfully applied in enantioselective radical cyalization[15,16], hydroalkylation[17,23-27], hydroamination[18], hydrosulfonylation[21,27,28] of olefins, and cross-electrophile coupling[20]. Most recently, Huang accomplished enantioselective photoenzymatic C(sp^2)-H functionalization through the single-electron oxidation of electron-rich arenes and alkenes[29,30] with low oxidation potentials (e.g., 3-methoxythiophene at +1.42V vs. the saturated calomel electrode (SCE))[31] (Fig. 1b). However, electron-deficient C(sp^3)-H bonds present significant challenges for direct oxidation[32], and their high bond dissociation energy (BDE) further limits C-H bond cleavage. For instance, the BDE of the C-H bond in malononitrile is as high as 87 kcal/mol[33]. Therefore, developing a novel strategy for the photoenzymatic enantioselective functionalization of electron-deficient C(sp^3)-H bonds is of great scientific importance.

We noticed that in the Bamford-Stevens reaction, diazo compounds can be transformed into carbonium ions in protic solvents[34], which might provide a theoretical basis for the generation of carbon-centered free radicals from diazo compounds via proton-coupled electron transfer (PCET)[35-37]. In light of this, we propose that generating ions as intermediates for radical formation could effectively facilitate reactions with substrates that do not readily form radicals. Building on this concept, we developed a cooperative photoenzymatic system comprising an ene-reductase (ER) and an organophotoredox catalyst to achieve the asymmetric functionalization of electron-deficient C(sp^3)-H bonds. In the catalytic process, carbanions are generated under alkaline conditions and oxidized to radicals via an excited-state photocatalyst-induced

single-electron transfer (SET). Stereoselectivity is then accomplished via an enantioselective HAT step of prochiral intermediates mediated by ER (Fig. 1c). This photoenzymatic system not only addresses a synthetic challenge unmet by either traditional organocatalysis[38-41] or photoenzymatic catalysis but also introduces an emerging mechanism for radical formation, one that has been rarely reported in photo-redox catalysis.

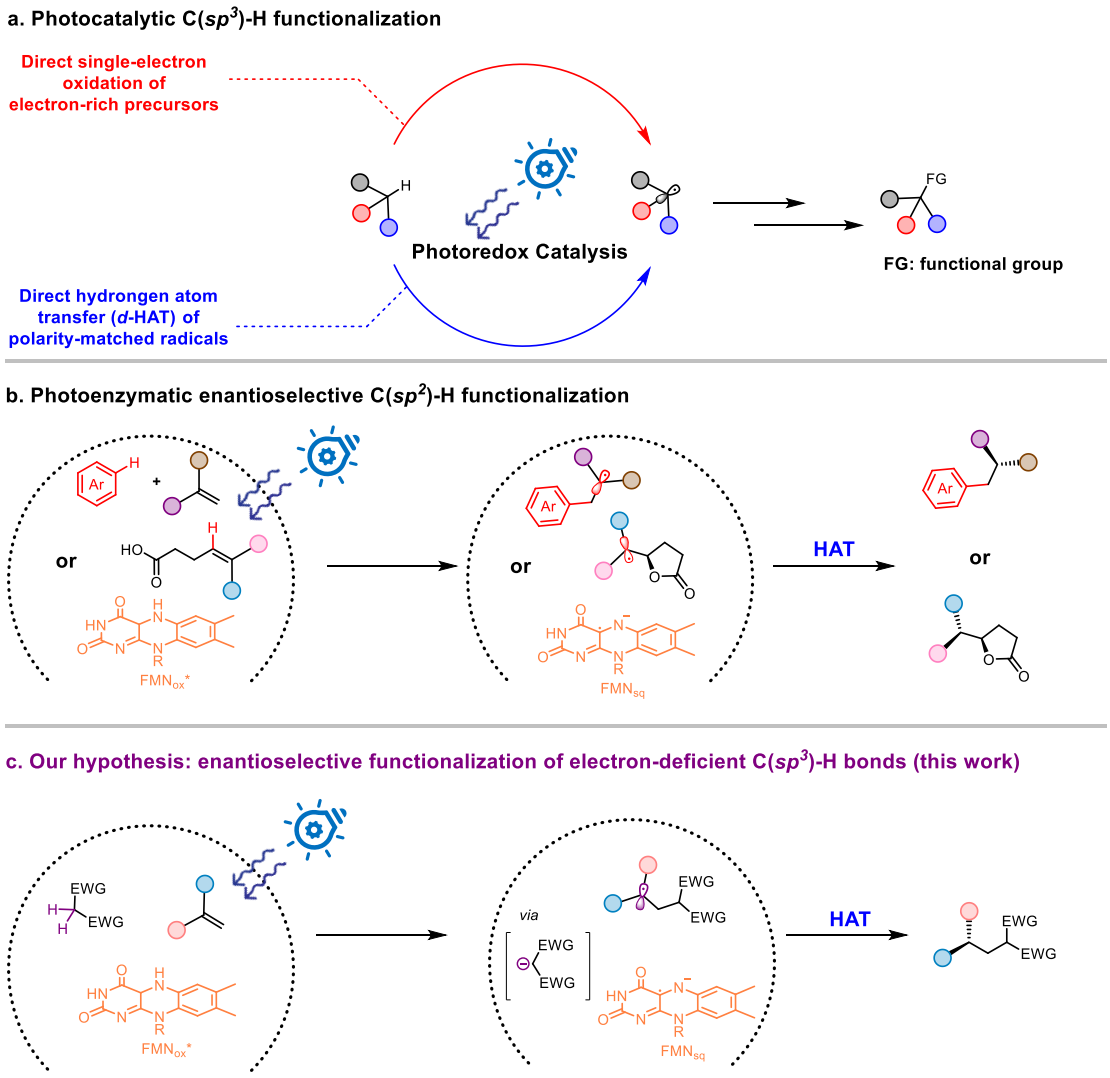

Fig. 1| Mode of photocatalytic C-H functionalization and our hypothesis.

Results and Discussion

Reaction development and engineering

Carbanions are rarely used as precursors for radical formation via single-electron oxidation in photoredox or photoenzymatic catalysis.[42] The main challenges is their high reactivity, which complicates regulating competition between single-electron oxidation and inherent activities like nucleophilic addition to unsaturated bonds[43]. Highly electrophilic radicals can also quickly convert into carbanions through radical polar crossover (RPC).[44] To develop a photoenzymatic system for the enantioselective functionalization of electron-deficient C(sp^3)-H bonds, suitable enzymes must remain active in alkaline conditions necessary for carbanion formation. The excited ER-FMN_{ox}^* must effectively oxidize carbanions into free radicals while minimizing undesirable pathways, such as carbanion nucleophilic addition, reductive quenching of FMN_{ox}^* by the reaction buffer or nearby amino acids, and RPC (Supplementary Fig. 6).

We investigated the proposed reactions using malononitrile **1a** and α-methylstyrene **2a** as model substrates with a library of ERs at 1 mol% under 455 nm blue LED illumination. Most ERs showed no catalytic activity (Table 1, entry 1 and Supplementary Table 3), but MorB, OYE2, SYE1, SYE2, SYE3, and GluER achieved yields of 1.2% to 3%. Notably, SYE2 and GluER exhibited the best and opposite enantioselectivity for **3a**. GluER had (*S*)-selectivity with a 4:96 enantiomeric ratio (er) (Table 1, entry 2), while SYE2 showed (*R*)-selectivity with a 93.3:6.6 er (Table 1, entry 3). Thus, SYE2 and GluER were chosen for further investigation.

To enhance the yield of **3a**, we tested various reaction conditions, including buffer systems, pH levels, and co-solvents (Supplementary Tables 4-5). Although these

adjustments did not significantly improve the yield, we decided to proceed with Tris buffer at pH 9 and ethanol as a co-solvent. Notably, the reaction only occurs at pH 9 or above, indicating that strongly alkaline conditions are essential for initiating carbanion formation in the catalytic cycle (Table 1, entries 4-6).

Unlike other photoenzymatic systems[28,29], adding extra FMN-Na did not enhance the yield of **3a** (Table 1, entry 7). This suggests that FMN_{ox}^{*}-induced single-electron oxidation of carbanions may be the rate-limiting step, indicating the need for photocatalysts with higher oxidative potential. We screened 18 transition metal and organic photocatalysts (Supplementary Tables 6-7) and identified fluorescein (FI-PC7), PC9, and PC12 as effective, increasing the yield of **3a** to 27%, 21%, and 19%, respectively, in both SYE2 and GluER-catalyzed reactions. The combination of 5 mol% FI with 1 mol% SYE2 or GluER gave the highest yields of **3a**, at 47.8% and 45.5%, respectively, without compromising enantioselectivity (Table 1, entries 8-9). Control experiments without light or in the presence of air did not produce the target product (Table 1, entries 10-11), supporting the visible-light-induced radical mechanism. Although neither FMN nor FI alone could catalyze the transformation (Table 1, entries 12-13), combining 10 mol% of both resulted in a 3% racemate of **3a** (Table 1, entry 14). These findings indicate that FI and FMN cooperate to catalyze the C(sp^3)-H functionalization process, highlighting the essential role of photoenzymes in improving efficiency and controlling the stereochemistry of radical processes.

Table 1 | Optimization of reaction conditions for photoenzymatic enantioselective C(sp^3)-H functionalization.

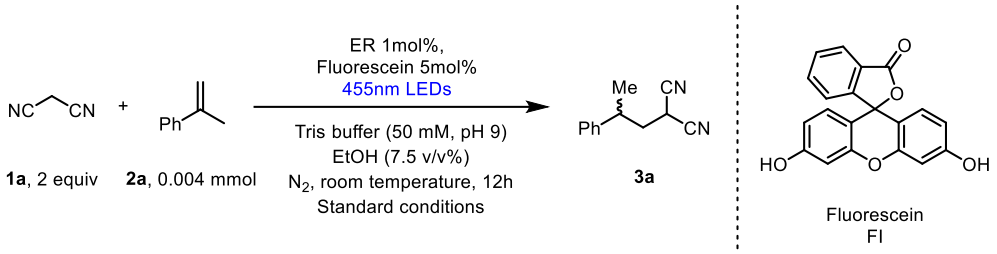

Entry	ER	Deviation from standard conditions[a]	Yield (%)[b]	er (%) (R:S)[c]
1	ERs[d]	w/o FI	n.r.	n.a.
2	GluER	w/o FI	1.3	4:96
3	SYE2	w/o FI	2.6	93.3:6.6
4	SYE2	Tris buffer pH 7.4, w/o FI	n.r.	n.a.
5	SYE2	Tris buffer pH 8, w/o FI	n.r.	n.a.
6	SYE2	Tris buffer pH 10, w/o FI	1.5	85:13
7	SYE2	w/o FI, 10 mol% FMN-Na	2.6	93.3:6.6
8	**SYE2**	**None**	**47.8**	**95.6:4.4**
9	**GluER**	**None**	**45.5**	**1.2:98.8**
10	SYE2	Dark	n.r.	n.a.
11	SYE2	Air	n.r.	n.a.
12	/	FMN-Na instead FI	n.r.	n.a.
13	/	None	n.r.	n.a.
14	/	10 mol% FMN-Na + FI	3	racemate

[a]Conditions: the total volume of standard reaction was 400 uL. [b]Yield was determined by gas chromatography. c er was determined by HPLC analysis on a chiral stationary phase, and the absolute configuration was established by theoretical calculations of electronic circular dichroism (ECD); see Supplementary Fig. 31 and Fig. 32. [d]LacER, KYE1, OYE1, OYE3, OPR1, SYE4, TOYE and YqjM were tested. n.r. No reaction; n.a. Not applicable.

Substrate scope investigations

We explored the substrate scope using SYE2 (ER1) and GluER to access both enantiomers of the products. While both enzymes showed excellent enantioselectivity for **3a**, this decreased significantly for most derivatives (Supplementary Fig. 33). To address this, we engineered GluER using site-saturated mutagenesis. Molecular

docking of GluER's crystal structure with **1a** and **2a** identified key residues in the substrate channel and FMN binding region, including T36, W66, H172, N175, Y177, T231, Q232, P239, R261, F269, and Y343 (see Supplementary Fig. 2). Site-saturated mutagenesis of these 11 sites led to GluER-Y343A (ER2), which showed improved enantioselectivity for both **3a** (up to R:S = 99.5:0.5) and other derivatives (Fig. 2).

The photoenzymatic system enabled hydroalkylation of various substituted methyl styrenes with functional groups at the para-/meta-/ortho positions of the phenyl group (**3a-j**), producing stereodivergent products with moderate to good yields and up to >1:99 er. Although 1-bromo-2-(prop-1-en-2-yl)benzene (**3k**) had a relatively low yield, it exhibited good to excellent enantioselectivity. Additionally, 2-naphthyl (**3l**), benzothiophene (**3m**), and biphenyl (**3n**) demonstrated the compatibility of photoenzymatic catalysis with aromatic rings and heterocycle. Variations at the α position of styrene had minimal impact on outcomes, as seen with **3p**. However, replacing aromatic olefins with aliphatic olefins significantly reduced the yield of **3o**. Although the mutant GluER-W66Q-Y343A (ER3) improved the yield of **3o**, the enantioselectivity remained unsatisfactory. Beyond malononitrile **2a**, dimethyl malonate **2b** could also alkylate with **3q** with excellent enantioselectivity. Moreover, this photoenzymatic catalysis can be successfully scaled up to 1 mmol with minimal changes in yield and enantioselectivity.

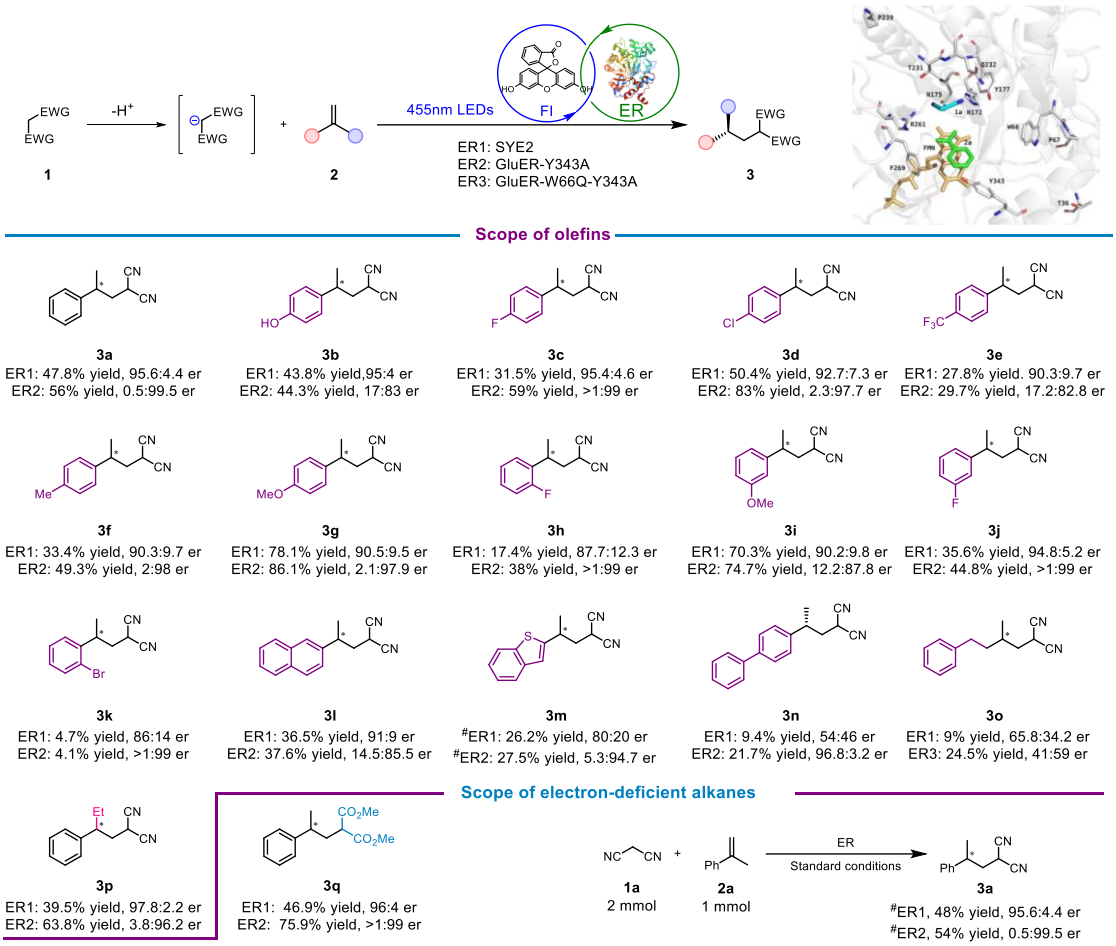

Fig. 2 | Substrate scope of enantioselective functionalization of electron-deficient C(*sp*^{3})-H bonds via hydroalkylation catalyzed by cooperative photoenzymatic system. Conditions: 1 (0.008 mmol), 2 (0.004 mmol), ER (1 mol%), FI (5 mol%), and EtOH (7.5 v/v%) in Tris buffer (50 mM, pH 9) were stirred at room temperature for 12 hours under N_2 with 455 nm LEDs. The total reaction volume was 400 μL. Yields were determined by gas chromatography, and the er by HPLC on a chiral stationary phase. # Isolated yield was obtained by scaling up the reaction.

Mechanistic investigations

Based on the experimental results, we proposed a synergistic photoredox and biocatalytic mechanism for new-to-nature photoenzymatic C(*sp*^{3})-H functionalization (Fig. 3a and detailed in Supplementary Fig. 22). In this catalytic cycle, malononitrile **1a** is first deprotonated in alkaline solutions to form carbanion intermediate **Int. A**. The

179 light-excited photocatalyst FI^* then oxidizes **Int. A** via SET, producing malononitrile
180 free radical **Int. B** and fluorescein radical anion $FI^{-\bullet}$. **Int. B** subsequently attacks α-
181 methylstyrene **2a**, forming a C-C bond and generating prochiral radical intermediate
182 **Int. C**, alongside FMN_{sq} from FMN_{ox} capturing an electron from $FI^{-\bullet}$. Finally, **Int. C**
183 undergoes ER-mediated enantioselective HAT, yielding enantioenriched **3a**, while
184 $FMNH^{\bullet}$ is oxidized back to FMN_{ox}, completing the catalytic cycle.

185 Several experiments were performed to support the proposed mechanism. The
186 photophysical properties of SYE2 and FI were measured to identify visible-light-
187 excited species. UV-vis absorption spectra show that SYE2 and FI absorb in the ranges
188 of 400-520 nm and 420-530 nm, with maximum absorptions at 460 nm and 490 nm,
189 respectively (Fig. 3b). This confirms that FI can be effectively excited by 455nm LED
190 to initiate the catalytic cycle. Stern-Volmer luminescence quenching experiments also
191 support the initial reductive quenching of excited FI^* by **1a** (**Int. A** → **Int. B**), as the
192 fluorescence intensity of FI decreased upon adding **1a**, unlike with **2a** (Supplementary
193 Fig. 10).

194 Several experiments were also performed to verify the generated radical
195 intermediates. Firstly, the radical trapping experiment was performed by adding 2
196 equivalents of 2,2,6,6-tetramethylpiperidine-1-oxyl (TEMPO) to the reaction mixture
197 under standard conditions. Only trace amounts of **3a** were detected, as the prochiral
198 radical intermediate **Int. C** was trapped by TEMPO, confirmed by high-resolution mass
199 spectrometry (HRMS) (Fig. 3c). Additionally, when α-cyclopropyl styrene **4** was
200 subjected to the photoenzymatic system, the ring-opening product **5** was observed as

the major product, supporting the involvement of **Int. C** (Fig. 3d). To further investigate the photo-oxidation step and clarify the resulting radical intermediates, electron paramagnetic resonance (EPR) experiments were conducted. With 5,5-dimethyl-1-pyrroline *N*-oxide (DMPO) as a radical trapping agent, slight changes in EPR signals were observed in the presence of **1a** compared to **2a** (Fig. 3b), indicating the formation of a potential **1a**-derived radical (**Int. B**), consistent with quenching experiments. The difference in EPR signals with and without **2a** suggests that the malononitrile radical **Int. B**, generated from the single-electron oxidation of the unstable carbanion **Int. A**, rapidly reacts with **2a** to form a more stable prochiral benzyl radical **Int. C** before being captured.[45]

Since apo-SYE2 (SYE2 without FMN) and FI alone did not catalyze the product formation, and adding extra FMN restored reactivity, we confirmed that the catalytic cycle requires the cooperative action of ER_FMN and FI (Fig. 3e and detailed in Supplementary Table 8 and Fig. 17). Finaly, deuterium-labelling experiments were conducted to investigate the final termination step (Fig. 3f). Using a deuterated buffer, the hydrogen at the stereogenic center was labelled at 76% D, suggesting that water may be involved in HAT steps.

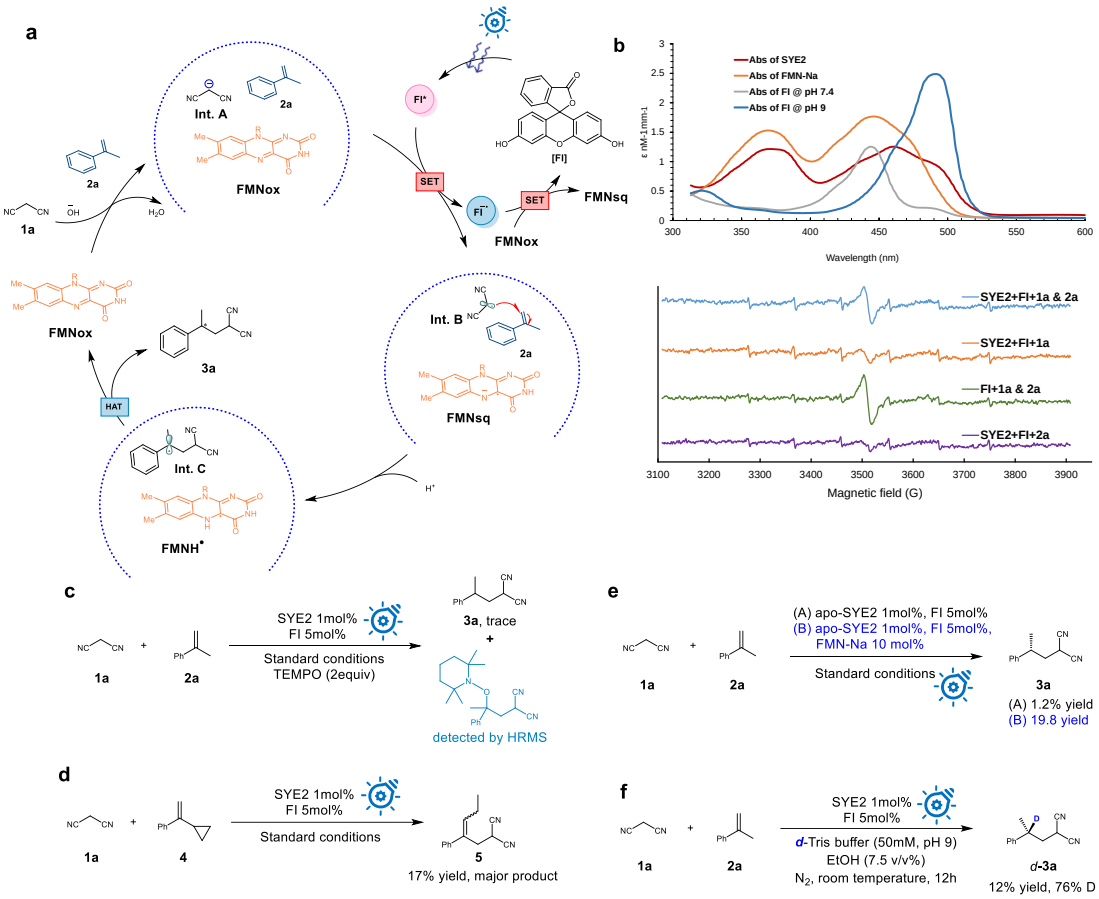

Fig. 3 | Mechanistic experiments and proposed catalytic cycle. a, Proposed catalytic cycle. **b**, UV-vis absorption (abs) spectra and room-temperature EPR experiments. **c**, TEMPO trapping experiment. **d**, Radical clock experiment. **e**, Photoenzymatic reactions catalysed by apo-flavoprotein. **f**, Deuterium-labelling experiment.

Computational studies

Extensive computational studies were performed to rationalize the mechanism proposed in Fig. 3a. Using hybrid cluster-continuum (HCC) model calculations, we found that **1a** undergoes facile deprotonation by OH^- ions in aqueous solution, forming the anionic species **Int. A.** with a low energy barrier of 0.3 kcal/mol (Supplementary Figure 20). To ascertain that **Int. A**, rather than **1a**, serves as the reactant for the generation of the carbanion intermediates **Int. B**, density functional theory (DFT)

231 calculations and time-dependent DFT (TD-DFT) calculations were conducted. The
232 Gibbs reaction energy (ΔG) for the excited FI^*-mediated oxidation of **1a** and **Int. A**
233 were calculated to be +105.2 kcal/mol and -32.1 kcal/mol (Fig. 4a and Supplementary
234 Fig. 15), respectively, supporting that photoinduced single-electron oxidation process
235 occurs through carbanion intermediates **Int. A**.

236 Since EPR experiments with FI, **1a**, and **2a** revealed distinctive radical signals,
237 suggesting that the formation of **Int. C** might be independent on ER participation.
238 Quantum mechanics (QM) model calculations show that the radical addition between
239 **Int. B** and **2a** has an energy barrier of 3.0 kcal/mol and an exothermicity of 10.7
240 kcal/mol (Fig. 4b), suggesting that formation of **Int. C** is quite facile. In addition,
241 deuteration experiments and the pKa value of FMN_{sq} (~8.5) suggested that the
242 protonation of FMN_{sq} to form neutral $FMNH^{\bullet}$ is feasible at pH 9, with a Gibbs reaction
243 energy (ΔG) of ~0.7 kcal/mol. Starting from $FMNH^{\bullet}$, HAT from $FMNH^{\bullet}$ to **Int. C** is
244 expected to yield the final product **3a**.

245 To elucidate the opposing enantioselectivity of GluER and SYE2, **Int. C** and FI
246 were docked into the enzyme active sites. Molecular dynamics (MD) simulations
247 indicate that FI was stabilized by Arg261 in GluER (Supplementary Fig. 23). **Int. C**
248 adopts two distinct conformations (CH_3-left and CH_3-right) in GluER, corresponding
249 to the *R* and *S* configurations, respectively. Moreover, the quantum mechanics
250 /molecular mechanics (QM/MM)-calculated HAT barriers are 16.2 kcal/mol for the
251 CH_3-right and 23.2 kcal/mol for the CH_3-left, aligning with the observed dominant
252 product (*S*)-**3a** (Fig. 4c and Fig. 4d). This is likely due to steric repulsion between the

bulky-CN substituent of **Int. C** and $FMNH^{\bullet}$ in the CH_3-left conformation, which tends to enlarge the distance between the C3 atom of **Int. C** and the N5-H of $FMNH^{\bullet}$ (4.10 Å in CH_3-left vs. 3.44 Å in CH_3-right), thereby increasing the energy barrier for HAT in CH_3-left conformation.

Unlike GluER, MD simulations reveal that the bulky-CN substituents in the CH_3-left conformation of **Int. C** forms a stable hydrogen bond with Tyr180 in SYE2, which positions bulky-CN away from $FMNH^{\bullet}$ and facilitates the subsequent HAT process, that is favor of generating (*R*)-**3a** (Supplementary Fig. 26). Indeed, our calculations suggest that the HAT process in SYE2 involves a barrier of 17.2 kcal/mol in the CH_3-left conformation and 22.0 kcal/mol in the CH_3-right conformation, leading to the dominant formation of (*R*)-**3a** that agrees with experiments (Supplementary Fig. 26 and Fig. 27).

Furthermore, the newly formed $FI^{-\bullet}$ could reduce FMN_{ox} to FMN_{sq} and release the initial ground state FI. DFT calculations show that $FI^{-\bullet}$ has the lowest redox potential among all functional photocatalysts (PC1, PC2, PC5, FI, PC10, and PC12), making it highly prone to transfer an electron to FMN_{ox} to form FMN_{sq} (Supplementary Fig. 16). This suggests that ET between FMN_{ox} and $FI^{-\bullet}$ enhances the whole catalytic process, explaining why FI is the most effective among all tested photocatalysts.

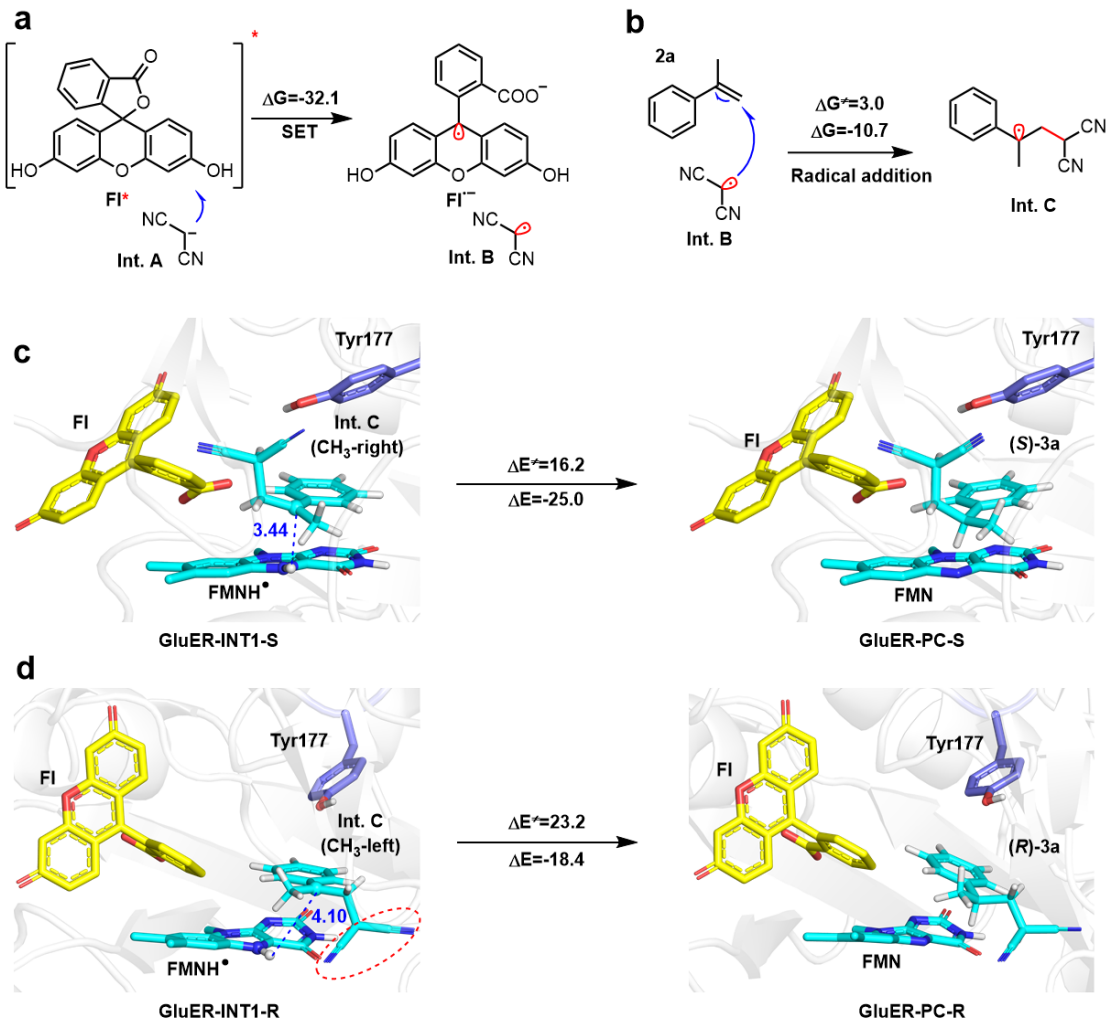

Fig. 4 | Mechanistic studies. a. SET from the excited FI^* to **Int. A**. **b**, The radical addition reaction between **Int. B** and **2a. c**, QM/MM-calculated energy of the HAT process from $FMNH^{\bullet}$ to the **Int. C** (CH_3-right) result in the production of *S*-(**3a**). **d**, QM/MM-calculated energy of the HAT process from $FMNH^{\bullet}$ to the **Int. C** (CH_3-left) result in the production of *R*-(**3a**).

Conclusions

In summary, we have developed a synergistic photoenzymatic system for the enantioselective functionalization of electron-deficient C(sp^3)-H bonds through radical intermediates generated by photoinduced single-electron oxidation of carbanions. This

281 enantiodivergent strategy, demonstrated in 17 cases with enantiomeric ratios up
282 to >1:99 and yields of up to 83%, offers potential for the one-step construction of
283 dicyano and diester compounds with remote stereocenters. Detailed mechanistic
284 experiments confirmed that the excited-state photocatalyst FI^* performs single-electron
285 oxidation of carbanion rather than directly oxidizing the electron-deficient
286 malononitrile **1a** to generate free radical intermediates. Unlike previous
287 photoenzymatic systems, the ET between the additional photocatalyst FI and FMN_{ox}
288 ensures catalytic cycle's smooth operation. This novel mode of photoenzymatic
289 catalysis is expected to inspire new strategies for forming free radical intermediates and
290 enabling new-to-nature biotransformation.
291

292 **Methods**

293 **General procedure for photoenzymatic reactions**

294 Taking **1a** + **2a** → **3a** as an example, in a glovebox (O_2 concentration <5 ppm), ,
295 solutions of ene-reductase (1 mol%), FI (10 μL, 2 mM stock in EtOH, 5 mol%), and
296 substrates mix (20 μL, 400 mM **1a** and 200 mM **2a** in EtOH) were added to a 4 mL vial
297 containing a magnetic stir bar and Tris buffer (50 mM, pH 9). The total volume of the
298 reaction mixture was 400 μL and the final concentrations for EtOH was 7.5%. The vial
299 was sealed with a screw cap, removed from the glove box, illuminated with blue LEDs,
300 and stirred for 12 h with a cooling fan (see Supplementary Fig. 3 for reaction setup).
301 For the reaction where the yield was determined by gas chromatography (GC), EtOAc
302 (1.0 mL) and 10.0 μL of an internal standard stock (20 mg/mL of n-dodecane in EtOAc)

were added to the reaction mixture and mixed thoroughly. For the reaction where the yield was determined by reverse phase HPLC, MeCN (1.0 mL) and 10.0 μL of an internal standard stock (16.8 mg/mL of 1,3,5-trimethoxybenzene in MeCN) were added to the reaction mixture and mixed thoroughly. The organic phase was separated and then analyzed by GC (or reverse phase HPLC), GC-MS and chiral HPLC. Product formation was confirmed by comparing retention times in GC/HPLC, as well as mass spectra and ^{1}H-NMR spectra of the crude material with those of the reference. Yield determined by GC was relative to the n-dodecane internal standard, while yield determined by reverse phase HPLC was relative to the 1,3,5-trimethoxybenzene internal standard. Enantioselectivity was determined by chiral HPLC.

System setup and MD simulations

The initial wild-type structure of GluER, was constructed based on the crystal structure (PDB code: 6O08). The SYE2 enzyme structure was modeled using AlphaFold2, and the position of FMN was confirmed by superimposing it with the GluER enzyme. Then, the **Int. C** and FI were docked into the active sites using AutoDock Vina tool. 100 ns MD simulations under the NPT ensemble. All MD simulations were performed with GPU version of Amber 18 package.

QM/MM calculations for enzymatic reactions

A representative snapshot extracted from the clustering results in the MD trajectory was used for subsequent QM/MM calculations. All QM/MM calculations were performed

using ChemShell combining Turbomole for the QM region and DL_POLY for the MM region. The electronic embedding scheme was used to account for the polarizing effect of the enzyme environment on the QM region.In all QM/MM geometry optimizations, the QM region was treated with the B3LYP functional using the double-zeta basis set def2-SVP for all atoms (labeled as B1). The energies were further corrected with the larger basis set def2-TZVP for all atoms (labeled as B2). Grimme's D3BJ empirical dispersion was included in all calculations.

DFT Calculations

All DFT calculations were performed with the Gaussian 16, Revision A.03 software. The initial structures were first optimized in conjunction with the SMD continuum solvation model at the B3LYP-D3/6-31G(d) level of theory. The solvation energies were further calculated at the M052X/6-31G* for all atoms. In particular, the solvent of water was used to simulate the reaction system.

TDDFT Calculations

The initial structures were first optimized at B3LYP/6-31G(d) level. Then, the single-point TDDFT calculations at wB97XD/6-311+G(d,p) levels were performed to compute the three low-lying singlet excited states. All TDDFT calculations were performed with Gaussian 16, Revision A.03.

Reporting summary

Further information on research design is available in the Nature Portfolio Reporting Summary linked to this article.

Data availability

Data relating to the materials and methods, experimental procedures, mechanistic studies and computational calculations, HPLC spectra, and NMR spectra are available in the Supplementary Information or from the authors on reasonable request. The atomic coordinates of the optimized computational models are available in the Supplementary Data.

References

1. Yamaguchi, J., Yamaguchi, A. D. & Itami, K. C-H bond functionalization: emerging synthetic tools for natural products and pharmaceuticals. *Angew. Chem. Int. Ed.* **51**, 8960-9009 (2012).

2. Leibler, I. N. M., Tekle-Smith, M. A. & Doyle, A. G. A general strategy for C(sp^3)-H functionalization with nucleophiles using methyl radical as a hydrogen atom abstractor. *Nat. Commun.* **12**, 6950-6959 (2021).

3. Li, Y., Lei, M. & Gong, L. Photocatalytic regio- and stereoselective C(sp^3)-H functionalization of benzylic and allylic hydrocarbons as well as unactivated alkanes. *Nat. Catal.* **2**, 1016-1026 (2019).

4. Bellotti, P., Huang, H.-M., Faber, T. & Glorius, F. Photocatalytic late-stage C-H functionalization. *Chem. Rev.* **123**, 4237-4352 (2023).

5. Capaldo, L., Ravelli, D. & Fagnoni, M. Direct photocatalyzed hydrogen atom transfer (HAT) for aliphatic C-H bonds elaboration. *Chem. Rev.* **122**, 1875-1924 (2022).

6. Yi, H. et al. Recent advances in radical C-H activation/radical cross-coupling. *Chem. Rev.* **117**, 9016-9085 (2017).

7. Miyake, Y., Nakajima, K. & Nishibayashi, Y. Visible-light-mediated utilization of α-aminoalkyl radicals: addition to electron-deficient alkenes using photoredox catalysts. *J. Am. Chem.Soc.*, **134**, 3338-3341 (2012).

8. Loh, Y. Y. et al. Photoredox-catalyzed deuteration and tritiation of pharmaceutical compounds. *Science* **358**, 1182-1187 (2017).

9. Cai, C.-Y., et al. Photoelectrochemical asymmetric catalysis enables site- and enantioselective cyanation of benzylic C-H bonds. *Nat. Catal.* **5**, 943-951 (2022).

10. Shaw, M. H., Shurtleff, V. W., Terrett, J. A., Cuthbertson, J. D. & MacMillan, D. W. C. Native functionality in triple catalytic cross-coupling: sp^3 C-H bonds as latent nucleophiles. *Science* **352**, 1304-1308 (2016).

11. Xu, A., Guo, J.-J., Pan, H. & Zuo, Z. Selective functionalization of methane, ethane, and higher alkanes by cerium photocatalysis. Science 361, 668-672 (2018).

12. Lei, G., Xu, M., Chang, R., Funes-Ardoiz, I. & Ye, J. Hydroalkylation of unactivated olefins via visible-light-driven dual hydrogen atom transfer catalysis. *J. Am. Chem. Soc.* **143**, 11251-11261 (2021).

13. Nagib, D. A. Asymmetric catalysis in radical chemistry. *Chem. Rev.* **122**, 15989-15992 (2022).

14. Mondal, S. et al. Enantioselective radical reactions using chiral catalysts. *Chem. Rev.*

122, 5842-5976 (2022).

15. Biegasiewicz, K. F. et al. Photoexcitation of flavoenzymes enables a stereoselective radical cyclization. *Science* **364**, 1166-1169 (2019).

16. Black, M. J. et al. Asymmetric redox-neutral radical cyclization catalysed by flavin-dependent 'ene'-reductases. *Nat. Chem.* **12**, 71-75 (2020).

17. Fu, H. et al. Ground-state electron transfer as an initiation mechanism for biocatalytic C-C bond forming reactions. *J. Am. Chem. Soc.* **143**, 9622-9629 (2021).

18. Ye, Y. et al. Using enzymes to tame nitrogen-centred radicals for enantioselective hydroamination. *Nat. Chem.* **15**, 206-212 (2023).

19. Gao, X., Turek-Herman, J. R., Choi, Y. J., Cohen, R. D. & Hyster, T. K. Photoenzymatic synthesis of α-tertiary amines by engineered flavin-dependent 'ene'-reductases. *J. Am. Chem. Soc.* **143**, 19643-19647 (2021).

20. Fu, H., et al. An asymmetric sp^3-sp^3 cross-electrophile coupling using 'ene'-reductases. *Nature* **610**, 302-307 (2022).

21. Chen, X. et al. Photoenzymatic hydrosulfonylation for the stereoselective synthesis of chiral sulfones. *Angew. Chem. Int. Ed. Engl.* **62**, e202218140 (2023).

22. Chen, B. et al. Modular access to chiral amines via imine reductase-based photoenzymatic catalysis. *J. Am. Chem. Soc.* **20**, 14278-14286 (2024).

23. Huang, X. et al. Photoenzymatic enantioselective intermolecular radical hydroalkylation. *Nature* **584**, 69-74 (2020).

24. Li, M., Harrison, W., Zhang, Z., Yuan, Y. & Zhao, H. Remote stereocontrol with azaarenes via enzymatic hydrogen atom transfer. *Nat. Chem.* **16**, 277-284 (2024).

25. Huang, X. et al. Photoinduced chemomimetic biocatalysis for enantioselective intermolecular radical conjugate addition. *Nat. Catal.* **5**, 586-593 (2022).

26. Li, M., Yuan, Y., Harrison, W., Zhang, Z. & Zhao, H. Asymmetric photoenzymatic incorporation of fluorinated motifs into olefins. *Science* **385**, 416-421 (2024).

27. Shi, Q. et al. Single-electron oxidation-initiated enantioselective hydrosulfonylation of olefins enabled by photoenzymatic catalysis. *J. Am. Chem. Soc.* **146**, 2748-2756 (2024).

28. Jiang, L. et al. Photoenzymatic redox-neutral radical hydrosulfonylation initiated by FMN. *ACS Catal.* **14**, 6710-6716 (2024).

29. Zhao, B. et al. Direct visible-light-excited flavoproteins for redox-neutral asymmetric radical hydroarylation. *Nat. Catal.* **6**, 996-1004 (2023).

30. Yu, J. et al. Repurposing visible-light-excited ene-reductases for diastereo-and enantioselective lactones synthesis. *Angew. Chem. Int. Ed. Engl.* **63**, e202402673 (2024).

31. Chen, B.-H., Du, Y.-D. & Shu, W. Organophotocatalytic regioselective C-H alkylation of electron-rich arenes using activated and unactivated alkenes. *Angew. Chem. Int. Ed. Engl.* **61**, e202200773 (2022).

32. Poudel, D. P., Pokhrel, A., Tak, R. K., Shakar, M. & Giri, R. Photosensitized O_2 enables intermolecular alkene cyclopropanation by active methylene compounds. *Science* **381**, 545-553 (2023).

33. Goebbert, D. J., Velarde, L., Khuseynov, D. & Sanov. A. C-H bond dissociation energy of malononitrile. *J. Phys. Chem. Lett.* **1**, 792-795 (2010).

34. Bayless, J. H., Friedman, L., Cook, F. B. and Shechter, H. Effect of solvent on the course of the Bamford-Stevens reaction. *J. Am. Chem. Soc.* **90**, 531-533 (1968).

35. Huang, X., Webster, R. D., Harms, K & Meggers, E. Asymmetric catalysis with organic azides and diazo compounds initiated by photoinduced electron transfer. *J. Am. Chem. Soc.* **138**, 12636-12642 (2016).

36. Duan, X. et al. A photoenzymatic strategy for radical-mediated stereoselective hydroalkylation with diazo compounds. *Angew. Chem. Int. Ed. Engl.* **62**, e e202214135 (2023).

37. Gu, Y.-J., Luo, M.-P., Yuan, H., Liu, G.-K. & Wang, S.-G. Photocatalytic enantioselective radical cascade multicomponent Minisci reaction of β-carbolines using diazo compounds as radical precursors. *Adv. Sci.* **11**, 2402272 (2024).

38. Guo, H., Fan, Y., Sun, Z., Wu, Y. & Kwon, O. Phosphine organocatalysis. *Chem. Rev.* **118**, 10049-10293 (2018).

39. Ni, H., Chan, W.-L. & Lu, Y. Phosphine catalyzed asymmetric organic reactions. *Chem. Rev.* **118**, 9344-9411 (2018).

40. Zhu, Z., Hu, Q., Fu, Y., Tong, Y. & Zhou, Z. Design and evolution of an enzyme for the asymmetric Michael addition of cyclic ketones to nitroolefins by enamine catalysis. *Angew. Chem. Int. Ed. Engl.* **63**, e202404312 (2024).

41. Cruz, P. D. J, Cassels, W. R., Chen, C.-H. & Johnson, J. S. Doubly stereoconvergent crystallization enabled by asymmetric catalysis. *Science* **376**, 1224-1230 (2022).

42. Yamashita, Y., Ogasawara, Y., Banik, T. & Kobayashi, S. Photoinduced efficient catalytic α-alkylation reactions of active methylene and methine compounds with

nonactivated alkenes. *J. Am. Chem. Soc.* **145**, 23160-23166 (2023).

43. Northrup, A. B. & MacMillan, D. W. C. The first direct and enantioselective cross-aldol reaction of aldehydes. *J. Am. Chem. Soc.* **124**, 6798-6799 (2002).

44. Tian, J. & Zhou, L. Photoredox radical/polar crossover enables C-H gem-difunctionalization of 1,3-benzodioxoles for the synthesis of monofluorocyclohexenes. *Chem. Sci.* **14**, 6045-6051 (2023).

45. Bowry, V. W. & Inlgold, K. U. Kinetics of nitroxide radical trapping. 2. Structural effects. *J. Am. Chem. Soc.***114**, 4992-4996 (1992).

Acknowledgements

This work was supported by the National Key R&D Program of China (2022YFA0912000), the Center of Synthetic Biology and Integrated Bioengineering (WU2022A006, WU2022A007, WU2023A009), the Research Center for Industries of the Future (WU2022C032). We thank Instrumentation and Service Center for Molecular Sciences (ISCMS) at Westlake University for the assistance in measurement and data interpretation. We thank Dr. Yinjuan Chen for the assistance with high resolution mass spectrometry (HRMS), Dr. Yuan Chen for the assistance with circular dichroism (CD), and Danyu Gu for the assistance with electron paramagnetic resonance (EPR).

Author contributions

J.Z. and Y.W. conceived and designed the overall project. J.Z. performed all synthetic

experiments and wet mechanism experiments. T.G., X.L., and M.-Z.M. created mutations. Q.Z., and X.W. carried out the computational studies and the calculation of absolute configuration (ECD) under the supervision of B.W. B.C. completed the calculation of redox potentials and Gibbs reaction energy (ΔG) for SET of Int. A. M.-J.M. performed the purification of some GluER variants. J.Z., B.W., and Y.W. wrote the paper with input of all authors.

Competing interests

The authors declare no competing interests.